Hindawi
Advances in Civil Engineering
Volume 2018, Article ID 3956509, 12 pages
https://doi.org/10.1155/2018/3956509

Research Article

Horizontal Loading Tests on Disconnected Piled Rafts and a Simplified Method to Evaluate the Horizontal Bearing Capacity

Xiao-jun Zhu[1,2] **Kang Fei**[1] **and Sheng-wei Wang**[1]

[1]*College of Civil Science and Engineering, Yangzhou University, Yangzhou 225127, Jiangsu, China*
[2]*School of Civil Engineering, Southeast University, Nanjing 210096, Jiangsu, China*

Correspondence should be addressed to Xiao-jun Zhu; zhuxiaojun@yzu.edu.cn

Received 24 April 2018; Revised 21 June 2018; Accepted 14 August 2018; Published 16 September 2018

Academic Editor: Chiara Bedon

Disconnected piled raft (DPR) foundations have been widely adopted as an effective foundation system where the piles are separated from the raft by a granular layer, which can limit the shear forces and moments transmitted between the raft and the piles. Thus, DPR foundations may avoid the problem of horizontal forces, such as those from an earthquake or dynamic loads, which damage the structural connection between the pile head and raft. A series of static horizontal loading tests were carried out on three types of foundation models, i.e., piled raft, disconnected piled raft, and raft alone models, on fine sand using a geotechnical model in a 1 g field. In this paper, the influences of vertical loading and interposed layer thickness were presented and discussed. The results showed that most of the horizontal force was carried by raft/interposed layer friction in the DPR foundation type, and the shear force and moment of the piles were greatly reduced due to the gap between the raft and the heads of the piles. The tested foundations were simulated using a simplified method with theoretical equations derived by making several approximations and assumptions. The simulated results agreed well with the test results.

1. Introduction

In situations where a raft foundation alone does not satisfy the design requirements, it may be possible to enhance the performance of a raft by adding piles, producing what is called a piled raft [1–3]. In seismically active zones, if the piles are structurally connected to the raft, high lateral shear forces and moments may develop at the connection between the piles and raft due to cyclic or dynamic horizontal loads. Meanwhile, the bearing capacity of the pile may be governed by their structural capacity rather than by their geotechnical capacity. Therefore, the concept of a disconnected piled raft has been discussed, where the piles are separated from the raft with an interposed granular load distribution layer [4, 5]. In such a foundation, the interposed layer prohibits loads that result from the superstructure in a direct manner, the disconnected piles are regarded as the ground reinforcement rather than pure structural members, and the factor of safety against structural failure can be significantly reduced. In addition, the disconnected piled raft avoids the problem of horizontal forces, such as those from earthquakes or dynamic loads, that can damage the structural connection between the pile head and raft since such forces can normally be resisted by the friction mobilized along the granular layer/raft contact, as shown in Figure 1.

Compared with the concept of piled raft foundations with connected piles, the disconnected piled raft alternative has been much less investigated. Some guidance was given by [4]. An analytical design method has been developed in the French research programme ASIRI. In addition, some piled footing projects have employed disconnected piled rafts. Among others, the Rion–Antirion Bridge in Greece [6, 7] and the ICEDA nuclear waste storage facility [8] were founded on clay reinforcement by settlement-reducing piles with an interposed granular load distribution layer, which can limit the shear forces and moments transmitted between the raft and the subsoil. However, the behaviour of the DPR under a seismic load has not been well clarified, which is partly due to the uncertainty in the complicated behaviour of the disconnected piled raft when it is subjected to seismic and lateral loads.

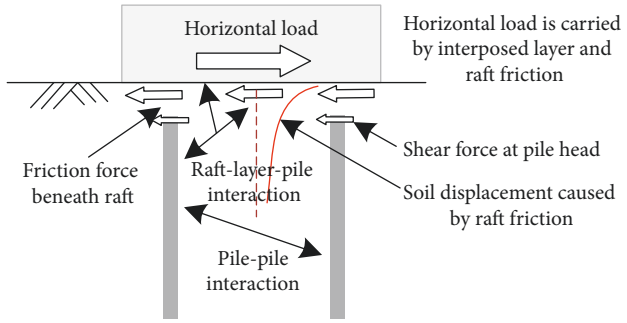

Figure 1: Horizontal load distribution within the disconnected piled raft foundations under a horizontal load.

To clarify the complicated behaviours of the disconnected piled raft, understanding the observed data under seismic and lateral loading is crucial. However, when comparing the studies of vertically loaded disconnected piled rafts, research on the behaviour of laterally loaded DPRs is relatively limited. Fatahi et al. [9, 10] found that the cushion could modify the dynamic structural characteristics and the load transfer mechanism and proved the seismic performance of the DPR foundation system using numerical software FLAC3D. In particular, the field data on disconnected piled raft foundations subjected to seismic and lateral loading are very limited. The behaviours of piled raft foundations recorded at the Pacific coast during the Tohoku earthquake [11] and the 2015 Nepal earthquake [12] are very rare case records. It was found that there was little change in the foundation settlement and the load sharing between the raft and the piles before and after the earthquake. But the horizontal accelerations of the superstructure were reduced to approximately 30% of those of the ground near the ground surface by the input losses due to the kinematic soil-foundation interaction in addition to the base isolation system [11].

Since it is difficult to record the actual field data of the piled raft foundation during an earthquake, physical models can play an important role in the study of connected or disconnected piled raft foundations under seismic or horizontal loading. Table 1 summarizes the research on piled raft models subjected to a static lateral load. A series of horizontal loading tests on piled raft models was conducted by [20]; in which a horizontal load was applied to the connected piled raft to discuss the pile bending moment and the shear force of the raft. Hamada et al. [13, 14] carried out static cyclic lateral loading tests on large-scale piled raft foundations and found that most of the lateral force was carried by raft friction when there was large contact earth pressure beneath the raft, and piles experienced pulling forces from the raft, behaving like anchors at large deformations. Sawada et al. [15] carried out a series of static horizontal loading tests by using a geotechnical centrifuge and found that the horizontal resistance of the pile part in the piled raft is higher than those observed in the pile group due to the raft base contact pressure. In their study, the piles were rigidly fixed to the raft.

In the above research, the influences of the connection between the pile head and raft were not considered. Matsumoto et al. [17, 18] carried out static and dynamic horizontal loading tests on a connected model piled raft to prove that the resonant frequency of superstructure decreases when the connection between the raft and the piles is hinged. Horikoshi et al. [19, 21] found that the horizontal stiffness of the piled raft with the hinged pile head connection was smaller than that of the piled raft with the rigid pile head connection, and the inclination of the piled raft during shaking was much smaller than that of the pile group due to the contribution of the soil resistance beneath the raft. Nakai et al. [16] focused on the connection conditions between the raft and piles subjected to dynamic loads by performing a centrifuge mode test and found that the dynamic response of a structure was reduced considerably by disconnecting the raft and pile. However, the detailed behaviour of disconnected piled raft foundations subjected to horizontal loads has yet to be clarified. This lack of clarification is partially because disconnected piled raft foundations are considered a raft foundation in the current design practice. Since the behaviour of a disconnected piled raft foundation subjected to horizontal or dynamic loads is considered fairly complex due to the interaction mechanisms among the raft, the granular layer, piles, and soil, the design procedure should include the effect of these mechanisms in an appropriate manner.

This paper examines the horizontal resistance of disconnected piled rafts. A series of static horizontal loading tests were conducted for a disconnected piled raft foundation to investigate the influence of vertical loading and the interposed layer thickness on the sectional forces on the piles. The most important issues in developing a seismic design concept for disconnected piled rafts are evaluating the sectional force on the piles and the lateral bearing capacity of the raft.

2. Horizontal Loading Tests

Static horizontal loading tests of raft foundations, piled raft foundations, and disconnected piled raft foundations were conducted in a 1 g field.

2.1. Testing Devices and Measuring Devices. The tests were conducted using a container indoors. The test arrangement for the disconnected piled raft foundation is shown in Figure 2. The container was 1.5 m long, 1.5 m wide, and 1.2 m high, and a piece of 20 mm thick transparent tempered glass existed on the front of the container, while the remaining four sides consisted of 10 mm thick steel plates. The horizontal load was applied using a fixed pulley device with a counterweight. The vertical load of the raft was applied by a jack over a tailor-made loading platform with steel balls to ensure that the raft was free to slide horizontally, and the footing was restrained from a rigid frame. To overcome the rigid ferrule effect on the soil container walls on soil, 25 mm thick foamed plastic was placed on the inner wall of the container to remove the soil level limit. During the test process, a layer of lubricating oil was applied to the inner wall of the tempered glass to reduce the friction between the test soil, half piles, and the box wall.

Table 1: Summary of previous studies on piled raft foundations subjected to a static horizontal load and this study.

	Loading condition	Condition between raft and pile head	Pile length (mm)	RVLP (%)	Foundation type tested
Hamada et al. [13]	Vertical load	Rigidly connected	700	45–82	R, PR, PG
Hamada et al. [14]	Vertical load	Rigidly connected	700	58–82	R, SP, PR, PG
Sawada et al. [15]	Vertical load	Rigidly connected	160	27	R, PR, PG
Nakai et al. [16]	Dynamic load	Connected and disconnected	180	0–100	PG, PR, DPR
Matsumoto et al. [17–18]	Vertical load	Hinged and rigidly connected	170	9.6–42.8	PR
Horikoshi et al. [19]	Vertical load	Hinged and rigidly connected	180	60	R, PR, SP
Pastsakorn et al. [20]	Vertical load	Rigidly connected	200	8.7–42.4	PR, PG
This study	Horizontal load	Disconnected	400	72–100	R, DPR

Note. RVLP is the proportion of the vertical load carried by the raft; *R* is the raft; PR is the piled raft; PG is the pile group; SP is the single pile; DPR is the disconnected piled raft.

The test device is mainly composed of a soil container, loading device, and measuring system. The measuring system consists of strain gauges, load cells, a data acquisition instrument, a linear displacement transducer (LDT), and a digital camera. The axial loads and bending moments on the piles were measured using strain gauges. Earth pressures beneath the raft and on top of the piles were measured using earth pressure cells.

2.2. Test Model Overview. Figure 2 shows the test setup including the model piled raft, model ground, and loading apparatus. Figure 3 shows the setup of the model piles prior to preparing the model ground and footing. The footing consisted of a high-strength steel plate that was 0.3 m long (B_r), 0.3 m wide, and 0.05 m deep placed on 9 piles including 3 half piles reinforced in the ground for disconnected piled raft foundations. The elasticity modulus of the raft footing was 3.2×10^5 MPa and can be considered as rigid because the raft-soil stiffness ratio is sufficiently high. The piles were disconnected from the steel footing. The piles were made from an aluminium pipe with a 20 mm outer diameter, 0.8 mm-thick wall, Young's modulus of 60000 MPa, and a second moment of area of 1.7×10^{-9} m^4. The piles were made not to be rigid and were 0.4 m long, which was longer than the footing width. The external layers of the piles and raft were specially treated via mechanical turning to ensure that the relative roughness of the pile-soil and raft-soil was greater than 0.1 so that the ultimate shear resistance did not depend on the raft surface roughness [22]. Both the length and the materials of the piles were selected based on the stiffness of the model sand. Strain gauges were attached inside the pile to measure the axial load along the pile. Pairs of shear strain gauges were attached to the opposite sides of the outer surface of each pile, which were wrapped by a silicone package to measure the bending moment and shear force. The half piles were affixed to the inside of the tempered glass as needed to take digital photographs, while piles P1, P2, P3, and P4 were regarded as the test piles.

2.3. Model Ground. The test soil samples are dry fine sand with 0.075–0.25 m size particles, and the interposed granular layer adopts gravel sand with a particle size between 0.5 mm and 5 mm. The particle size distributions of the soil samples and interposed layer are shown in Figure 4, and the physical properties of the model sand are summarized in Table 2. The internal friction angle estimated from consolidated drained tests was 32 degrees at a relative density of 60%. When filling in the sand, dry fine sand was poured in 10 cm thick layers into the container from a height of 2.2 m above the model ground surface. The sand weight from each layer can be calculated from the sand density and the volume of each layer. Stratified compaction was carried out until the soil reached the design height. The samples were not moved after laying the sand for 12 hours to ensure the consistency of the density under the pressure of gravity.

2.4. Test Series. The test cases were conducted in the order listed in Table 3. The piles were penetrated at a rate of 0.3 mm/s until the raft base reached the ground surface for the piled raft. With these installation processes, the piles in the piled raft and the disconnected piled raft foundations can be regarded as displacement piles. The test cases were focused on the thickness of the interposed layer and the vertical load to find the factors affecting the horizontal load transfer mechanism of the disconnected piled raft, while R1 and PR2 were used as reference tests. In the test, a vertical load was first exerted on the raft model, and a horizontal load was imposed later through the fixed pulley and counterweight after settling. In the trial test, when the vertical load applied on the raft was 800 N, the horizontal ultimate load of the raft reached 350 N; thus, the value of each loading step was taken as 50 N. For each loading stage, the static load was kept constant for 10 mins, and then data including the raft horizontal displacement record, the strain data of the pile shaft, and the Earth pressure load were gathered. Digital photographs were taken to record the soil deformation observation points and the soil displacement field.

3. Test Results and Analysis

Piles P1, P2, P3, and P4 were selected as the test piles. By measuring the tensile strain ε_+ and the compressive strain ε_- at each cross section of the pile shaft, the bending moments can be calculated by the following equation:

$$M = \frac{E_p I_p \Delta\varepsilon}{b_0}, \quad (1)$$

where M is the bending moment, E_p is the elastic modulus of the pile, I_p is the inertia moment of the pile section, b_0 is the

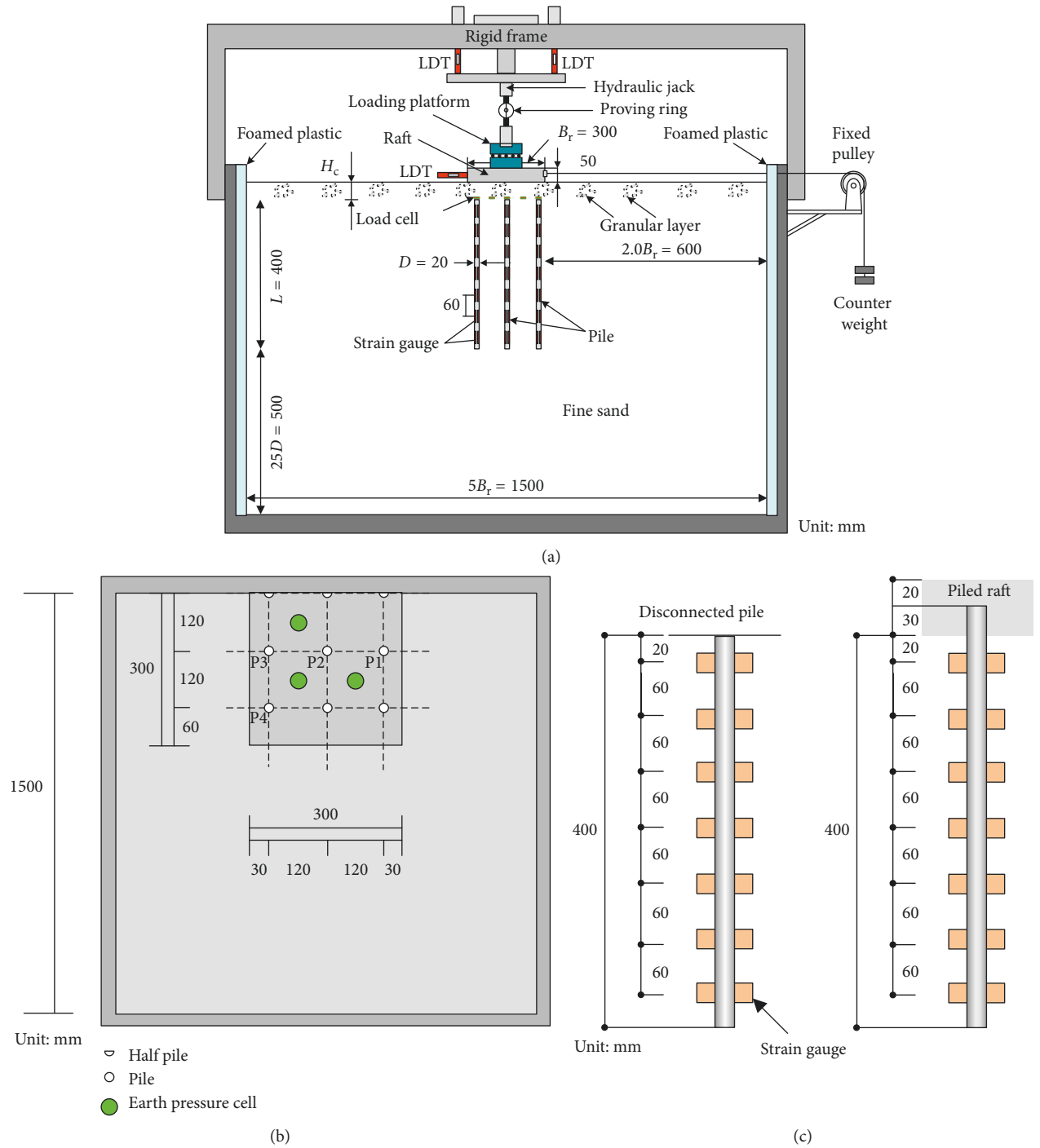

Figure 2: Sketch map of the test model. (a) Side view. (b) Top view. (c) Attached strain gauge arrangement.

space between the tensile strain and compressive strain, and $\Delta\varepsilon = \varepsilon_+ - \varepsilon_-$ is the bending strain of the pile section.

Then, dividing the difference between the two sectional moments by the distance between the two sections, the shear force of the piles can be obtained through the following equation:

$$Q = \frac{dM}{dz}, \tag{2}$$

where Q is the shear force of the piles and z is the depth of the pile section.

3.1. Raft Load-Displacement Curve. To study the behaviour of disconnected piled raft foundations under a lateral load, analyses of the raft and piled raft under a lateral load were performed as references. The total vertical load was proportional to the maximum lateral load of the raft foundation, as shown in Figure 5. The evaluated coefficient of friction was 0.44, calculated as the maximum horizontal load versus the vertical load in Figure 5.

Figure 6 shows the influence of the vertical loads and interposed layer thickness on the lateral response of the DPR

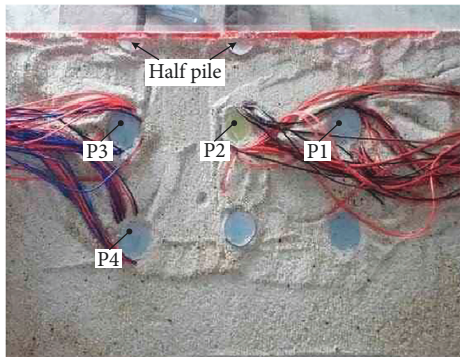

Figure 3: Sketch map of the piles.

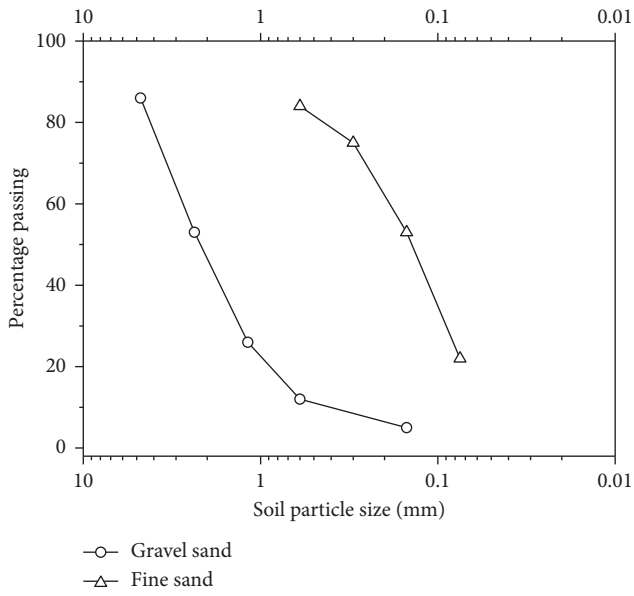

Figure 4: Particle-size distributions of soil in the model test.

Table 2: Physical properties of the model sand.

Sand types	Fine sand	Gravel sand
50 percent diameter D_{50} (mm)	0.12	2.37
Maximum density (g·cm^{-3})	1.67	1.72
Minimum density (g·cm^{-3})	1.42	1.38
Uniformity coefficient, C_u	2.81	2.13
Specific gravity of the soil particles	2.64	2.66
Relative density	0.6	0.67
Internal friction angle, φ (°)	32.23	34.14
Cohesion, c (kPa)	1.8	0.6
Compression modulus, E_s (MPa)	22	36

foundations in sandy soil. It can be illustrated that the lateral capacity of the DPR is affected by the presence of the vertical load but slightly affected by the thickness of the interposed layer. However, the largest displacement distance of the raft increased with the thickness of the interpose layer in DPR foundations. Compared to the DPR foundation, the displacement distance was restrained in the raft of PR2 and DPR6 due to the rigid connection of the pile-raft and vertical load.

3.2. Pile Bending Moment. Figure 7 illustrates the effects of the interposed layer on the bending moments of the piles. The bending moments have similar distributions along the piles. However, compared to the piled raft foundation, the deflection and the maximum moment of the piles of the DPR foundations are lower by 56–82% than those in PR2 due to the interposed layer. Meanwhile, the bending moment decreases with an increase in the interposed layer thickness.

Figure 8 examines the synergistic effects of a horizontal force and a vertical load applied simultaneously on the raft foundation. Three different vertical loads of 400 N, 800 N, and 1600 N are considered in this figure. The effect of the vertical load on the lateral responses of the pile is revealed in Figure 8. Compared with the 400 N vertical load, when the load increases to 800 N and 1600 N, the bending moment rises approximately 70% and 166%, respectively, which means the bending moment, particularly within its upper part, increases with the vertical load. This increase is because the greater the vertical load is, the greater the contact pressure between the bottom of the raft and the soil is, leading to greater frictional and horizontal forces delivered to the soil.

3.3. Pile Shear Force. Figure 9 exhibits the pile shear force distribution considering the interposed layer thickness, where PR2 is a reference. It can be seen that the maximum pile shear force appears at the top of the pile and gradually decreases with an increase in the depth. At a distance of 140 mm from the pile top (about seven times that of the pile diameter), the pile shear force becomes 0; if the distance is larger than 140 mm, then the reverse shear force comes out, which is the result of the soil round pile resistance on the piles. When the interposed layer thicknesses are 20 mm and 40 mm, the maximum shear forces at the pile top are 5.6 N and 11.3 N, respectively. However, the maximum shear force at pile top in PR2 is 52.1 N, so we can get a conclusion that the shear force at the pile top can be reduced significantly by the interposed layer between the pile head and raft. Otherwise, the shear force at the pile top decreases with the thickness of the interposed layer.

The effect of the vertical load on the lateral responses of the pile shear force is revealed in Figure 10. The results indicate that the shear force at the pile top increases with an increase in the vertical load. This law is consistent with the abovementioned law that the pile bending moment changes with vertical loading, as shown in Figure 8.

Based on the effect of the interposed layer thickness and the vertical load on the shear force at the pile top, as shown in Figure 11, it can be seen that the shear force decreases with the thickness of the interposed layer, while the shear force increases with an increase in the vertical load. In other words, the interposed layer can adjust the horizontal load sharing between the pile and soil through the mobility of the soil particles and shear deformation.

4. Soil Displacement Field

The soil displacement process during the horizontal loading tests was captured by a high-resolution camera. The analysis grid could be superimposed onto the photographs. The

Table 3: Test arrangement.

Case	Foundation type	Pile diameter, D (mm)	Pile space/pile diameter, S/D	Pile length, L (mm)	Interposed layer thickness, H_c (mm)	Vertical load, P (N)	Initial RVLP (%)
R1	Raft	—	—	—	—	800	100
PR2	Piled raft	20	6	400	—	800	72
DPR3	Disconnected piled raft	20	6	400	20	800	100
DPR4	Disconnected piled raft	20	6	400	40	800	100
DPR5	Disconnected piled raft	20	6	400	40	400	100
DPR6	Disconnected piled raft	20	6	400	40	1600	100

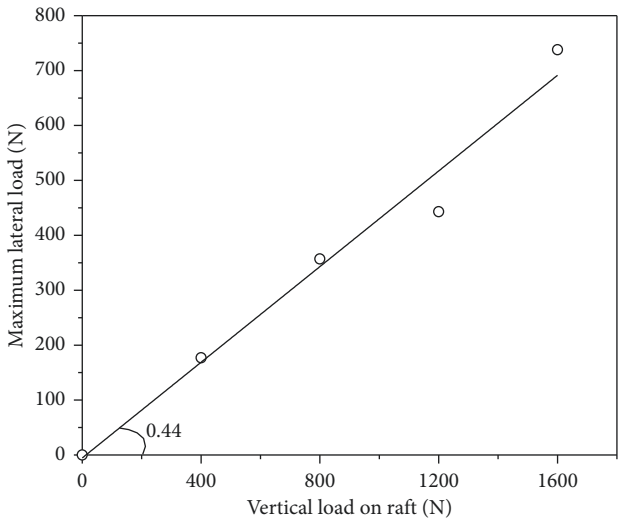

Figure 5: Load-displacement curve of the raft.

images have a resolution of 7.9 pixels per millimetre. Then, using MATLAB's toolbox for digital image correlation [23], it is possible to track the movement of the soil and compute the strain field that occurs in the soil mass.

4.1. Horizontal Displacement Field. The soil displacement field obtained from the digital image correlation (DIC) technique is shown in Figure 12. To visualize the soil displacement more easily, colour changes are defined in the colour bar. The interval for DPR6 was $0 <$ displacement value < 4.0. The unit of the coordinates is millimeter. During the initial loading, the displacement is mainly concentrated on the right region of the interposed layer, and there is a rather small displacement from the left side of the raft. With an increase in the horizontal load, the soil displacement field from the right side of the raft also increases continuously. Afterwards, the displacement field from the right region spreads along the lower right direction and forms a local displacement concentration area under the right side of raft, as shown in Figure 12(b).

Six characteristic particles (M1~M6) from the bottom of the raft are tracked based on the soil displacement nephogram, and the horizontal displacement curve is shown in Figure 13. In Figure 13, the dotted line is the horizontal displacement of measuring points M4, M5, and M6 under different horizontal loads; the solid line is the horizontal displacement of measuring points M1, M2, and M3. It can be seen that the horizontal displacement decreases with the depth of the measuring points. Meanwhile, the horizontal displacement from the right side of the raft is larger than that from the middle position. Additionally, the larger the horizontal load is, the more obvious the difference value is.

As the raft moves to the right, the soil from the left side, which was squeezed by the raft, losses the support from the raft blade and collapses, leading to the result that there exists a rather small horizontal displacement regarding the soil particles on the left side of the raft. In comparison, the soil particles on the right side of the raft experience were squeezed and displaced on the right, meaning that there exists a larger horizontal displacement for soil particles from the right bottom of the raft than that from the left bottom.

It is revealed that soil particles near the left side of the raft edge angle mainly generate a clockwise rotation, while those near the right side of the edge angle are rotated in the counterclockwise direction due to the pushing of raft, as shown in Figure 14. There exists an interface that connects the positive and negative corners in the particle movement system, where the particles rotate clockwise and counterclockwise alternatively and finally form a thorough soil shear zone.

4.2. Soil Shear Failure Band. Figure 15 presents the soil shear band diagram of the DPR foundations under a horizontal load when the vertical load is 1600 N and the thickness of interposed layer is 40 mm. It can be found that when the horizontal load is small, a number of independent shear bands start to form on the right side of the raft but do not become scalable; thus, the interposed layer still has a certain stability. As the horizontal load increases, the shear and deformation fields continue to develop, producing local shear zones that finally interpenetrate with each other to form complete shear bands.

5. Calculation Method of the Horizontal Bearing Capacity for the DPR Foundations

5.1. Simplified Calculation Model. Figure 16 is the load path diagram of the DPR foundations under both vertical and horizontal loads. Subjected to both vertical and horizontal

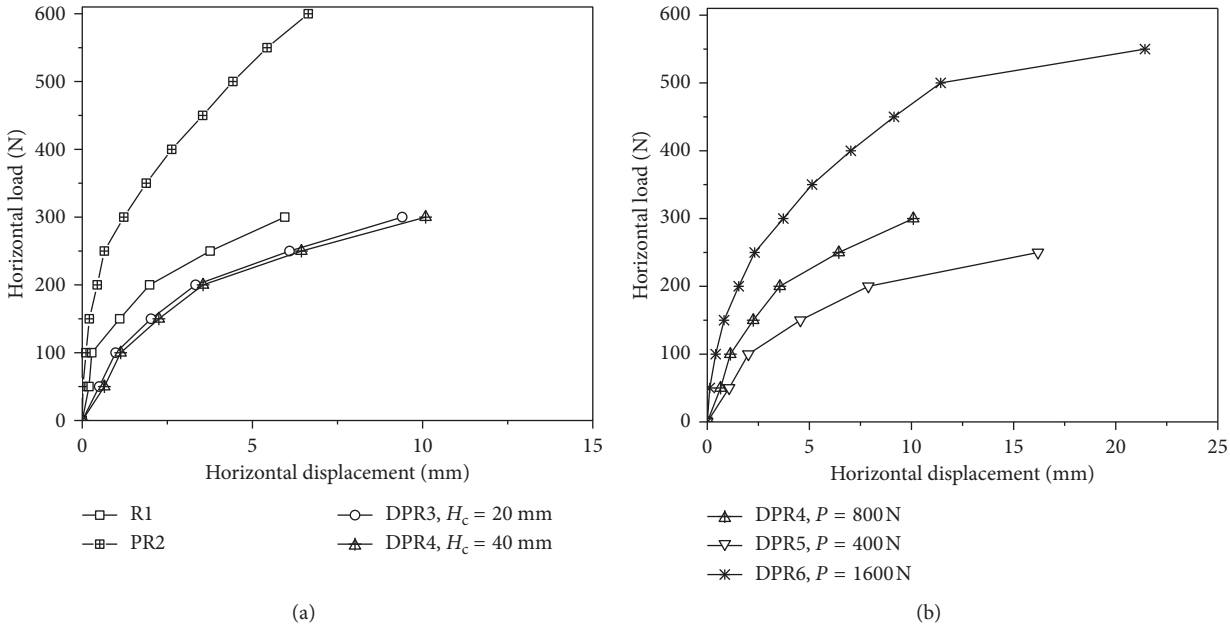

Figure 6: Horizontal load versus horizontal displacement of the raft foundations. (a) The influence of the connection condition between the raft and piles. (b) The influence of the vertical load on the DPR.

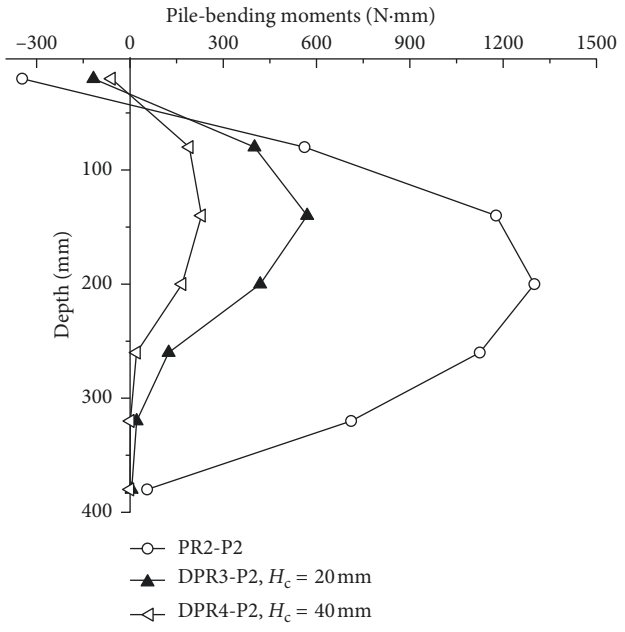

Figure 7: Influence of the interposed layer on the responses of the pile bending moments under a 300 N horizontal force.

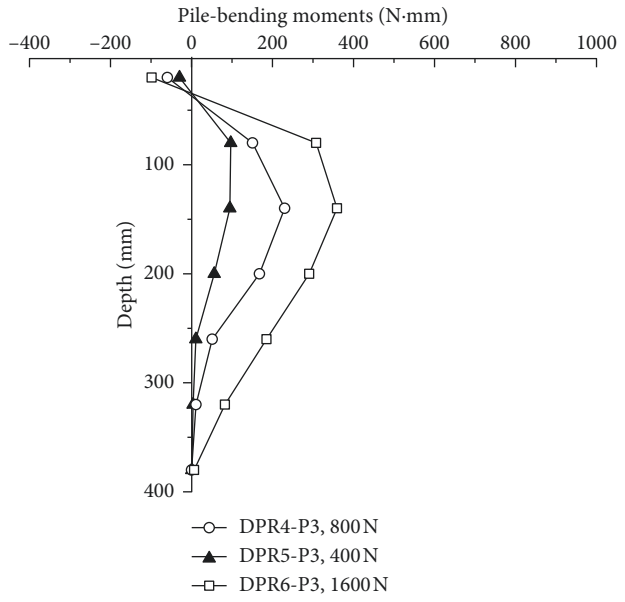

Figure 8: Influence of vertical loading on the lateral responses of the pile bending moments under a 300 N horizontal force.

loads on the raft, the raft will first transfer the load down to the interposed layer and the surrounding soil of the raft, and then later, the load will be passed to the pile and the soil between the piles.

According to the horizontal force transfer mechanism of DPR foundations, if the pressure distributed on the bottom of the raft is uniform and experiences vertical and horizontal load, then its horizontal bearing capacity is composed of the bearing capacity of the raft structure, the interposed layer, the interface between the raft and interposed layer, and the interface between the interposed layer and pile-soil ground. The minimum horizontal bearing capacity in each part can exert control over the DPR foundations, which means the calculation method for horizontal bearing capacity of the DPR foundations can be listed as

$$Q = \min\left(Q_R, Q_I, Q_{R-I}, Q_Z\right), \tag{3}$$

where Q is the horizontal bearing capacity of the DPR foundations, Q_R is the horizontal ultimate bearing capacity

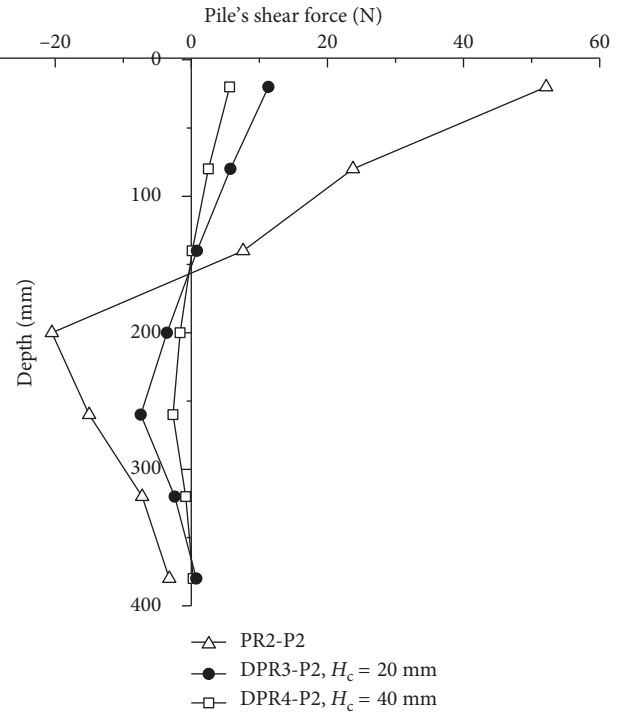

Figure 9: Influence of the interposed layer on responses of the pile shear force under a 300 N horizontal force.

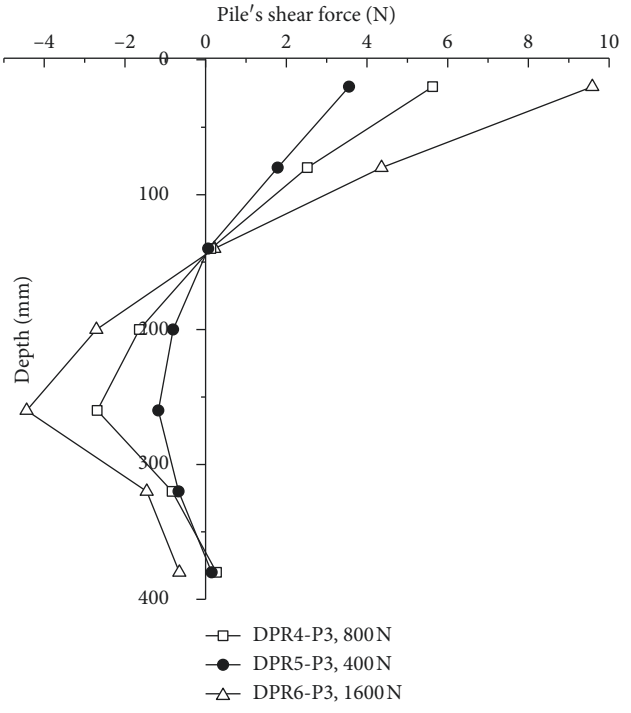

Figure 10: Influence of the interposed layer on the responses of the pile shear force under a 300 N horizontal force.

of the raft structure, Q_I is the horizontal ultimate shear bearing capacity of the interposed layer, Q_{R-I} is the horizontal bearing capacity of the interface between the raft and interposed layer, and Q_Z is the horizontal bearing capacity of the interface between the interposed layer and pile-soil ground.

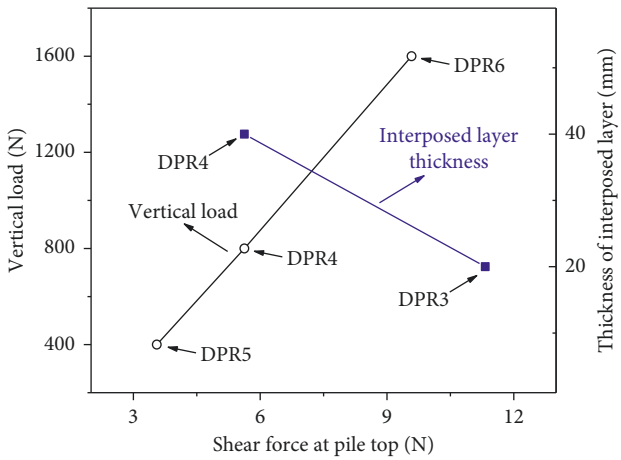

Figure 11: Shear force at the pile top versus interposed layer thickness and vertical load.

5.2. Theoretical Analysis of Horizontal Bearing Capacity

(1) The horizontal ultimate bearing capacity of the raft structure is decided by its own strength. Because the raft in this test is an absolute rigid body, its bearing capacity is considered large.

(2) Subjected to vertical and horizontal loads, the interposed layer appears as horizontal shear failure. Figure 17 shows the interposed layer cell form any points for analysis.

The major and minor principal stress is

$$\sigma_{1,3} = \frac{\sigma_x + \sigma_y}{2} \pm \sqrt{\left(\frac{\sigma_x - \sigma_y}{2}\right)^2 + \tau_x^2}, \quad (4)$$

where σ_1 is the major principal stress, σ_3 is the minor principal stress, σ_x is the x-stress, σ_y is the y-stress, and τ_x is the x-shear stress.

The angle between the principal stress plane and the horizontal plane is

$$2\alpha_0 = \arctan\left(\frac{-2\tau_x}{\sigma_x - \sigma_y}\right), \quad (5)$$

where α_0 is the angle between the principal stress plane and the horizontal plane.

The angle between the failure surface and the major principal stress plane is

$$\theta_f = 45 + \frac{\varphi}{2}, \quad (6)$$

where θ_f is the angle between the failure surface and the major principal stress plane and φ is the internal friction angle of the interposed layer.

Then, the angle between the failure surface and the horizontal plane is

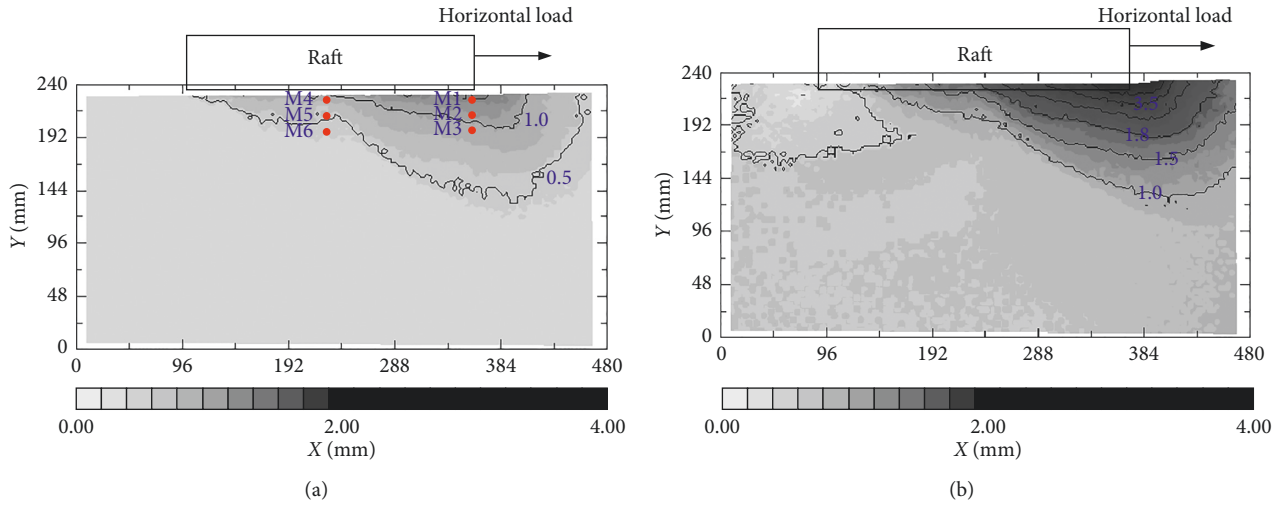

Figure 12: Soil displacement nephogram: horizontal load of (a) 100 N and (b) 500 N.

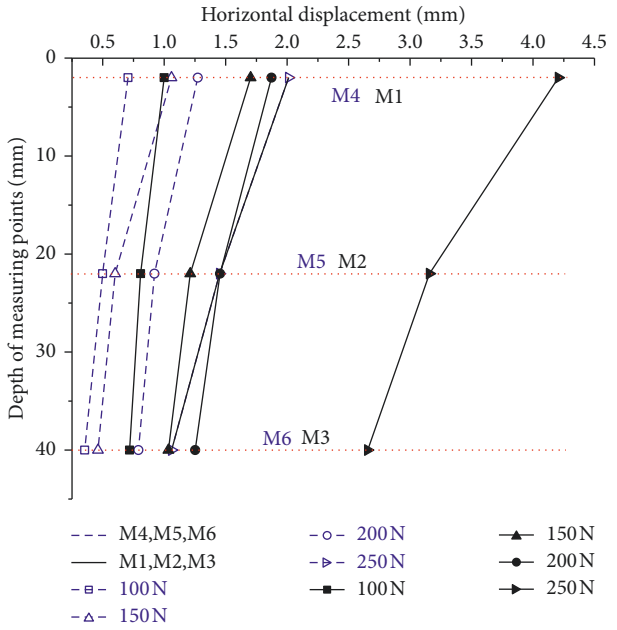

Figure 13: Horizontal displacement path of the characteristic particles.

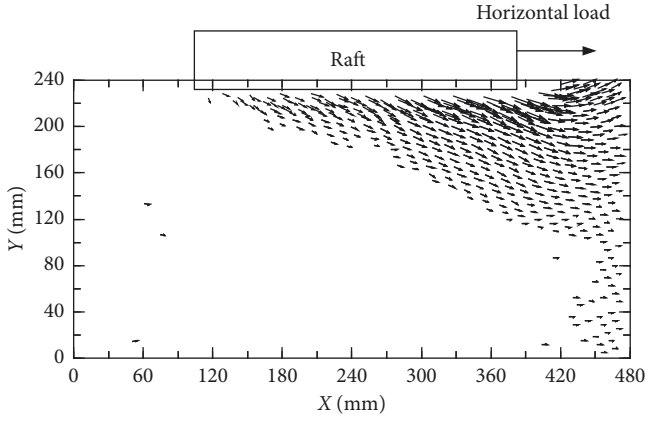

Figure 14: Vector diagram of soil particles in the displacement field.

$$\theta = 45 + \frac{\varphi}{2} + \frac{\arctan\left[\left(\sigma_x - \sigma_y\right) - \left(\sin\varphi + 2c \cdot \cos\varphi\right)^2\right]}{2}, \tag{7}$$

where θ is the angle between the failure surface and the horizontal plane and c is the cohesion of the soil.

If shear failure occurs to the interposed layer, then

$$\sigma_1 = \sigma_3 \cdot \frac{1 + \sin\varphi}{1 - \sin\varphi} + 2c \cdot \frac{\cos\varphi}{1 - \sin\varphi}. \tag{8}$$

From Equations (3) and (7), the maximum horizontal shear stress can be listed as

$$\tau_{\max} = \frac{\sqrt{\left[\left(\sigma_x + \sigma_y\right)\sin\varphi + 2c \cdot \cos\varphi\right]^2 - \left(\sigma_x - \sigma_y\right)^2}}{2}, \tag{9}$$

where $\tau_{\max}$ is the maximum horizontal shear stress; c is the cohesion of the interposed layer; σ_y is the vertical stress of the soil from the top of the interposed layer; and $\sigma_x = (\nu/1-\nu) \cdot \sigma_y$ is the horizontal stress of the soil from the top of the interposed layer, in which ν is referred to as Poisson's ratio of the interposed layer.

The horizontal ultimate shear bearing capacity of the interposed layer is

$$Q_l = \tau_{\max} \cdot S, \tag{10}$$

where S is the contact area of the raft with an interposed layer.

(3) The horizontal bearing capacity at the interface between the raft and interposed layer is mainly the frictional force generated between the raft bottom and the interposed layer under the influence of the horizontal sliding trend. Additionally, with passive earth pressure from the horizontal load direction, the

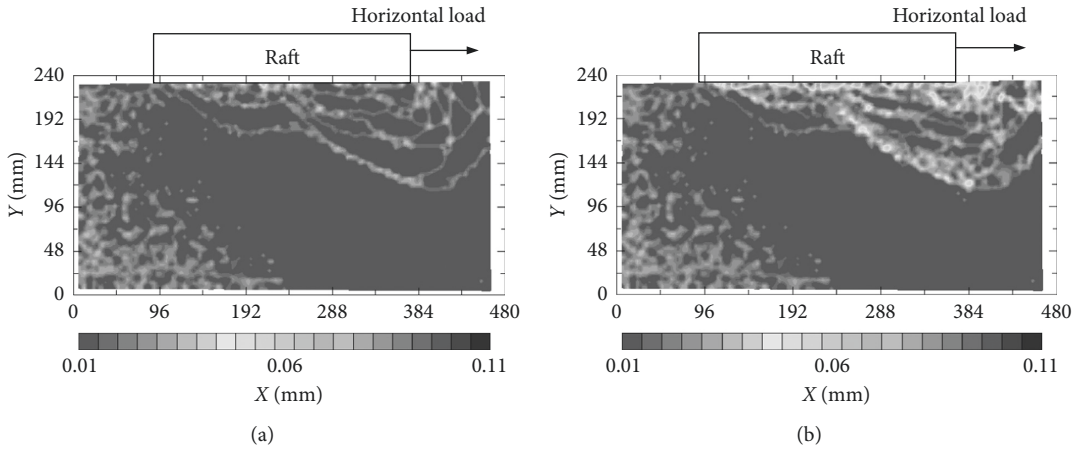

Figure 15: Soil shear band nephogram: horizontal load of (a) 100 N and (b) 500 N.

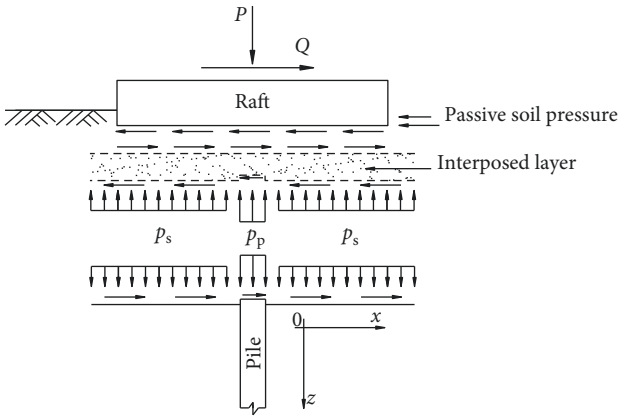

Figure 16: Horizontal force transfer mechanism of DPR foundations.

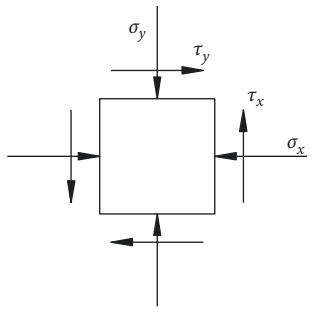

Figure 17: Model of the interposed layer cell.

calculation method of the horizontal bearing capacity is

$$Q_{R-I} = \mu_{R-I} \cdot (P + W_R) + E_p,$$
$$E_p = \frac{1}{2} \cdot \gamma H^2 K_p + 2c \cdot H\sqrt{K_p}, \tag{11}$$

where μ_{R-I} is the static friction coefficient between the raft and the interposed layer, γ is the soil unit weight, P is the vertical load undertaken by the raft, W_R is the weight of the raft, E_p is the passive earth pressure, K_p is the coefficient of the passive soil pressure, and H is the buried depth of the raft.

(4) The bearing capacity of interface between the interposed layer and pile-soil ground mainly includes the horizontal bearing capacity between the interposed layer and pile head and the capacity at the interface between the interposed layer and pile-soil, of which the calculation method can be listed as

$$Q_Z = Q_P + Q_S,$$
$$Q_P = \mu_{I-P} \cdot P_p = \mu_{I-P} \cdot \frac{P \cdot n \cdot m}{1 + m(n-1)}, \tag{12}$$
$$Q_S = \mu_{I-S} \cdot P_S = \mu_{I-S} \cdot \frac{P \cdot (1-m)}{1 + m(n-1)},$$

where Q_P is the horizontal bearing capacity between the interposed layer and pile head, Q_S is the horizontal bearing capacity between the interposed layer and soil, μ_{I-P} is the static friction coefficient between the interposed layer and pile head, $\mu_{I-S} = \tan((2/3) \cdot \phi)$ is the static friction coefficient between the interposed layer and soil (the external frictional angle is taken 1/2~2/3 of the internal frictional angle based on the empirical value), φ is the soil internal friction angle, n is the pile-soil stress ratio, and m is the pile replacement ratio.

5.3. Comparison of the Theoretical Calculation and Test Results. The theoretical calculation method proposed in this paper is used to calculate the horizontal bearing capacity of the tests DPR4 and DPR6. The calculated results were compared with the model test results to verify the applicability of the calculation method. The test parameters are listed as follows: self-weight of the raft, $W_R = 167N$; base area, $S = 0.09\ m^2$; buried depth of the raft, $H = 0.01$ m; replacement rate, $m = 0.01$; pile-soil stress ratio, $n = 3.56$; static friction coefficient between the raft and the interposed

Table. 4: Comparison of the calculation and test results on the horizontal bearing capacity of the DPR foundations.

Horizontal bearing capacity of the piled raft foundation with a cushion	Vertical load 800 N (DPR4)			Vertical load 1600 N (DPR6)		
	Test result (N)	Calculation result (N)	Relative error (%)	Test result (N)	Calculation result (N)	Relative error (%)
Raft, Q_R	350	—	—	500	—	—
Granular layer, Q_I	350	406.2	16.1	500	483.7	3.3
Interface between the raft and granular layer, Q_{R-I}	350	324.0	7.4	500	574.3	14.9
Interface between interposed layer and pile-soil ground, Q_Z	350	378.2	8.1	500	534.6	7.0

layer, $\mu_{R-I} = 0.42$; static friction coefficient between the interposed layer and the pile head, $\mu_{I-P} = 0.42$; and the static friction coefficient between the interposed layer and soil, $\mu_{I-S} = 0.39$. Other parameters are shown in Table 3. Table 4 presents the theoretical calculation results for the horizontal bearing capacity of the DPR foundations compared with the test data.

It can be concluded from Table 4 that when the vertical load is 800 N, the DPR's horizontal bearing capacity is controlled by the bearing capacity of the interface between the raft and interposed layer. However, the bearing capacity of the DPR foundations is controlled by the interposed layer's horizontal bearing capacity when the vertical load is 1600 N, which is consistent with the conclusion that foundation failure occurs at the interposed layer in the model test, as shown in Figure 15. When the thickness of the interposed layer is 40 mm, the vertical loads are 800 N and 1600 N, and the corresponding theoretical calculation results of the horizontal bearing capacity for the DPR foundations are $Q = \min(Q_R, Q_I, Q_{R-I}, Q_Z) = 324$ N and 483.7 N, respectively. Meanwhile, the measuring data in the model test are 350 N and 500 N with the relative error rates of 7.4% and 3.3%, respectively. In this sense, the calculation method put forward in this paper appears to be of some usefulness for theoretical calculations regarding the horizontal bearing capacities of DPR foundations.

6. Conclusions

In this paper, an experimental and theoretical study of the horizontal bearing capacity of DPR foundations was presented based on six laboratory tests. The focus of the study was on the thickness of the interposed layer and vertical load on the raft. The main conclusions of this study are as follows:

(1) Compared to the piled raft foundation, the deflection and the maximum moment of the pile of the DPR foundations are lower by 56–82% than those of PR2 due to the interposed layer.

(2) The pile shear force decreases with the thickness of the interposed layer, while the force increases with an increase in the vertical load. In other words, the interposed layer can adjust the horizontal load sharing between the pile and soil through the mobility of soil particles and shear deformation.

(3) The soil shear and deformation fields were reproduced by using the DIC technique. It was seen that a number of independent shear bands began to form on the right side of the raft but do not become scalable during the initiation of loading. Then, the local shear zones finally interpenetrated with each other to form complete shear bands at the later stage of the loading.

(4) A calculation method for horizontal bearing capacity of the DPR foundations was put forward, which is compared with the model test results to prove its correctness.

Data Availability

The data used to support the findings of this study are available from the corresponding author upon request.

Conflicts of Interest

The authors declare that they have no conflicts of interest.

Acknowledgments

This study was supported by the Natural Science Foundation of Jiangsu Province of China (Project nos. BK20170509 and BK20170501), the National Natural Science Foundation of China (Project no. 51778557), and the Natural Science of Foundation for Colleges and Universities in Jiangsu Province (Project no. 15KJB580013).

References

[1] H. G. Poulos, "Piled raft foundations: design and applications," *Géotechnique*, vol. 51, no. 2, pp. 95–113, 2001.

[2] O. Reul and M. F. Randolph, "Piled rafts in overconsolidated clay: comparison of in situ measurements and numerical analyses," *Géotechnique*, vol. 53, no. 3, pp. 301–315, 2003.

[3] A. Mandolini, G. Russo, and C. Viggiani, "Pile foundations: experimental investigations, analysis and design," in *Proceedings of the 16th ICSMGE*, pp. 177–213, Osaka, Japan, September 2005.

[4] H. Wong, M. F. Chang, and X. D. Cao, "Raft foundations with disconnected settlement-reducing piles. Thomas Telford," in *Design Application of Raft Foundations*, J. A. Hemsley, Ed., pp. 469–486, Thomas Telford, London, UK, 2000.

[5] V. Fioravante, "Load transfer from a raft to a pile with an interposed layer," *Géotechnique*, vol. 61, no. 2, pp. 121–132, 2011.

[6] J. Garnier and A. Pecker, "Use of centrifuge tests for the validation of innovative concepts in foundation engineering,"

in *Proceedings of the 2nd International Conference of Earthquake Geotechnical Engineering*, pp. 431–439, Lisboa, Portugal, June 1999.

[7] A. Pecker, "Design and construction of the rion antirion bridge," in *Proceedings of Geotechnical Engineering for Transportation Projects*, pp. 216–240, Los Angeles, CA, USA, July 2004.

[8] N. Mattsson, A. Menoret, C. Simon, and M. Ray, "Case study of a full-scale load test of a piled raft with an interposed layer for a nuclear storage facility," *Géotechnique*, vol. 63, no. 11, pp. 965–976, 2013.

[9] B Fatahi, S Basack, P Ryan et al., "Performance of laterally loaded piles considering soil and interface parameters," *Geomechanics and Engineering*, vol. 7, no. 5, pp. 495–524, 2014.

[10] R Xu and B Fatahi, "Geosynthetic-reinforced cushioned piles with controlled rocking for seismic safeguarding," *Geosynthetics International*, pp. 1–78, 2018.

[11] K. Yamashita, "Field measurements on piled raft foundations in Japan," in *Proceedings of the 9th International Conference on Testing and Design Methods for Deep Foundations (IS-Kanazawa)*, pp. 79–94, Kanazawa, Japan, December 2012.

[12] P. Badry and N. Satyam, "Seismic soil structure interaction analysis for asymmetrical buildings supported on piled raft for the 2015 Nepal earthquake," *Journal of Asian Earth Sciences*, vol. 133, no. 1, pp. 102–113, 2017.

[13] J. Hamada, T. Tsuchiya, T. Tanikawa, and K. Yamashita, "Lateral loading tests on piled rafts and simplified method to evaluate sectional forces of piles," *Geotechnical Engineering Journal of the SEAGS and AGSSEA*, vol. 46, no. 2, pp. 29–42, 2015.

[14] J. Hamada, N. Aso, A. Hanai, and K. Yamashita, "Stress of piles and lateral load sharing ratio between piles and raft evaluated from seismic observation on piled raft foundation," *Journal of Structural and Construction Engineering*, vol. 77, no. 680, pp. 1537–1544, 2012.

[15] K. Sawada and J. Takemura, "Centrifuge model tests on piled raft foundation in sand subjected to lateral and moment loads," *Soils and Foundations*, vol. 54, no. 2, pp. 126–140, 2014.

[16] S. Nakai, H. Kato, R. Ishida et al., "Load bearing mechanism of piled raft foundation during earthquake," in *Proceedings of the 3rd UJNR Workshop on Soil-structure Interaction*, pp. 29-30, Menlo Park, CA, USA, March 2004.

[17] T. Matsumoto, K. Fukumura, P. Kitiyodom, K. Horikoshi, and A. Oki, "Experimental and analytical study on behaviour of model piled rafts in sand subjected to horizontal and moment loading," *International Journal of Physical Modelling in Geotechnics*, vol. 4, no. 3, pp. 1–19, 2004.

[18] T. Matsumoto, K. Fukumura, K. Horikoshi, and A. Oki, "Shaking table tests on model piled rafts in sand considering influence of superstructures," *International Journal of Physical Modelling in Geotechnics*, vol. 4, no. 3, pp. 21–38, 2004.

[19] K. Horikoshi, T. Matsumoto, Y. Hashizume, T. Watanable, and H. Fukuyama, "Performance of piled raft foundations subjected to static horizontal loads," *International Journal of Physical Modelling in Geotechnics*, vol. 3, no. 2, pp. 37–50, 2003.

[20] K. Pastsakorn, Y. Hashizume, and T. Matsumoto, "Lateral load tests on model pile groups and piled raft foundations in sand," in *Proceedings of International Conference Physical Modelling in Geotechnics*, pp. 709–714, St John's, Canada, July 2002.

[21] K. Horikoshi, T. Matsumoto, Y. Hashizume, and T. Watanable, "Performance of piled raft foundations subjected to dynamic loading," *International Journal of Physical Modelling in Geotechnics*, vol. 3, no. 2, pp. 51–62, 2003.

[22] V Fioravante, "On the shaft friction modelling of non-displacement piles in sand," *Journal of the Japaness Geotechnical Society Soils and Foundation*, vol. 42, no. 2, pp. 23–33, 2002.

[23] E. Christoph, T. Robert, and G. Daniel, *Digital Image Correlation and Tracking with Matlab*, 2006.